

# Second-harmonic generation in the scattering of light by two-dimensional particles

Claudio I. Valencia and Eugenio R. Méndez

*División de Física Aplicada, Centro de Investigación Científica y de Educación Superior de Ensenada, Km. 107 Carretera Tijuana-Ensenada, Ensenada, B.C. 22860, Mexico*

Bernardo S. Mendoza

*Centro de Investigaciones en Óptica, Apartado Postal 948-1, 37000 León, Guanajuato, Mexico*

Received February 25, 2003; revised manuscript received June 20, 2003

A numerical technique for studying the generation of second-harmonic radiation in the interaction of light with two-dimensional particles of arbitrary shape is described. The medium of which the particles are composed is assumed to be homogeneous and isotropic. For the special case of cylindrical particles the numerical results are compared with results obtained with a Mie-type theory. The numerical technique is then illustrated through calculations for particles of various shapes by use of a free-electron model for nonlinear polarization. Among other things, we have found that, when a symmetrical particle is illuminated along its axis of symmetry, there is no second-harmonic radiation along that axis and that *s*-polarized second-harmonic light can be generated only by a mixture of *s*- and *p*-polarized illumination. The effects that the departure from cylindrical shape has on the resonances were also studied. © 2003 Optical Society of America

*OCIS codes:* 190.3970, 190.4350, 240.4350, 290.5850.

## 1. INTRODUCTION

In recent years, nonlinear optical techniques have become a standard means of probing the state of surfaces and interfaces. In particular, second-harmonic generation (SHG) is now established as a powerful spectroscopic tool for the study of the physical and chemical properties of the surfaces of centrosymmetric materials (see, e.g., the reviews in Refs. 1–4). The sensitivity of this nonlinear effect to the state of the surface is due to the fact that, within the dipole approximation, a centrosymmetric material does not produce second-harmonic radiation. At the surface, however, the inversion symmetry is broken, permitting a dipolar contribution to the harmonic field. The theoretical development of the field is an ongoing subject of research, and, on the experimental side, the availability of powerful and stable laser sources is making second-harmonic studies more accessible and facilitating their application to a wide range of systems.

Most of SHG studies, both theoretical and experimental, have been concerned with planar surfaces.<sup>1–12</sup> Recently, however, some attention has been given to nonlinear interactions between optical waves and rough, or nonplanar, surfaces.<sup>13–21</sup> These studies have been motivated partly by the need for understanding the interplay between multiple scattering and nonlinearities.

Recent advances in nanofabrication techniques permit the production of controlled systems of small particles, such as structured clusters, self-assembled particles, and quantum dots. The nonlinear optical properties of such structures can be used in the characterization of those structures and, more interestingly, are also becoming important in applications. Although some publications have dealt with SHG by small particles,<sup>22–27</sup> most treat-

ments are either restricted to particles smaller than the wavelength or based on simplified models of the nonlinearity.

In this paper we calculate the second harmonics generated by arbitrary-shaped two-dimensional particles. We do so by employing the undepleted-pump approximation (Ref. 28, p. 79), assuming that the medium is homogeneous and isotropic, and assuming that the surface of the particle is locally flat. In our approach the second-harmonic field is obtained through the numerical solution of integral equations satisfied by the source fields at the fundamental and harmonic frequencies. Interesting aspects of the technique are that it can be applied to two-dimensional particles of any shape and that the results can easily be extended to collections of particles.

The formulation is illustrated by calculations based on the free-electron model for nonlinear polarization.<sup>8,29–31</sup> We point out, however, that our results are not restricted to this case; they represent the general solution to the problem of SHG by particles of an isotropic and homogeneous material that are invariant along one direction, illuminated perpendicularly to that direction. We tested the numerical technique by comparing calculations for cylinders with the results of analytical work.<sup>32</sup> These theoretical tools were then used to study the scattering cross section, or efficiency, and the angular intensity distribution of the light generated at the harmonic frequency for particles of various shapes under different conditions of illumination.

The paper is organized as follows: First, in Section 2 we present some general results on the theory of SHG from surfaces and specialize them to surfaces or particles that are invariant in one direction. The numerical technique is described in Section 3. In Section 4 we calculate

some illustrative examples, employing a free-electron model for the nonlinear polarization, and, finally, in Section 5 we present our conclusions.

## 2. NONLINEAR SOURCES

Consider, for the moment, the locally flat interface shown in Fig. 1. It divides medium I, assumed to be vacuum, and nonlinear medium II. For the region below the interface, at the harmonic frequency, Maxwell's equations can be written in the form

$$\nabla \times \mathbf{E}(\mathbf{r}|2\omega) = \frac{2i\omega}{c} \mathbf{H}(\mathbf{r}|2\omega), \quad (1a)$$

$$\nabla \times \mathbf{H}(\mathbf{r}|2\omega) = -\frac{2i\omega}{c} \mathbf{D}(\mathbf{r}|2\omega), \quad (1b)$$

$$\nabla \cdot \mathbf{D}(\mathbf{r}|2\omega) = 0, \quad (1c)$$

$$\nabla \cdot \mathbf{H}(\mathbf{r}|2\omega) = 0. \quad (1d)$$

We also have the constitutive relation

$$\mathbf{D}(\mathbf{r}|2\omega) = \epsilon_{\text{II}}(2\omega)\mathbf{E}(\mathbf{r}|2\omega) + 4\pi\mathbf{P}^{\text{NL}}(\mathbf{r}|2\omega), \quad (2)$$

where  $\mathbf{P}^{\text{NL}}(\mathbf{r}|2\omega)$  represents the nonlinear polarization.

For isotropic media the first nonzero contribution to the bulk nonlinear polarization is given by the quadrupolar term. The third-order susceptibility tensor has 21 nonzero elements, of which only 3 are independent (see, e.g., Ref. 28, p. 48). Then the nonlinear polarization takes the general form<sup>1,3,8</sup>

$$\begin{aligned} \mathbf{P}^{\text{NL}}(\mathbf{r}|2\omega) = & \alpha[\mathbf{E}(\mathbf{r}|\omega) \cdot \nabla]\mathbf{E}(\mathbf{r}|\omega) \\ & + \beta\mathbf{E}(\mathbf{r}|\omega)[\nabla \cdot \mathbf{E}(\mathbf{r}|\omega)] \\ & + \gamma\nabla[\mathbf{E}(\mathbf{r}|\omega) \cdot \mathbf{E}(\mathbf{r}|\omega)], \end{aligned} \quad (3)$$

where  $\alpha = \delta - \beta - 2\gamma$ , and the constants  $\delta$ ,  $\beta$ , and  $\gamma$  are frequency-dependent parameters that characterize the medium. In a homogeneous medium the second term on the right-hand side of Eq. (3) must always vanish. Under excitation by a plane wave the first term also vanishes, but it must be kept for more-general illumination conditions.

To determine the boundary conditions it is convenient to introduce a local system of coordinates  $x$ - $y$ - $z$  with origin on the surface, in which the unit vectors  $\hat{x}$  and  $\hat{y}$  are

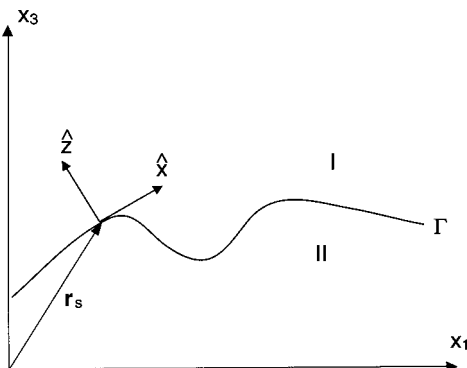


Fig. 1. Illustrative diagram of the local surface geometry.

tangential to the surface and  $\hat{z}$  is normal to the surface (see Fig. 1). Multiplying Eq. (1a) by  $\hat{z}$ , we can write

$$\frac{\partial \mathbf{E}_t(\mathbf{r}|2\omega)}{\partial z} = \nabla_t E_z(\mathbf{r}|2\omega) - \left(\frac{2i\omega}{c}\right) [\hat{z} \times \mathbf{H}_t(\mathbf{r}|2\omega)], \quad (4)$$

where the subscripts  $t$  and  $z$  indicate components that are tangent and normal to the surface, respectively. Integrating this expression along  $\hat{z}$ , we find that

$$\mathbf{E}_t^{(\text{I})}(\mathbf{r}_s|2\omega) - \mathbf{E}_t^{(\text{II})}(\mathbf{r}_s|2\omega) = -4\pi\nabla_t P_z^s(\mathbf{r}_s|2\omega), \quad (5)$$

where  $\mathbf{r}_s$  represents points on the surface and the superscripts (I) and (II) indicate evaluation from above and from below the interface, respectively. In writing Eq. (5) we defined the normal component of the surface nonlinear polarization as

$$P_z^s(\mathbf{r}_s|2\omega) = \lim_{\tau \rightarrow 0} \int_{-\tau}^{\tau} \frac{P_z^{\text{NL}}(\mathbf{r}_s, z|2\omega)}{\epsilon_{\text{II}}(z|2\omega)} dz. \quad (6)$$

Starting from Eq. (1b) and following a similar procedure, we find that

$$\mathbf{H}_t^{(\text{I})}(\mathbf{r}_s|2\omega) - \mathbf{H}_t^{(\text{II})}(\mathbf{r}_s|2\omega) = 4\pi \left(\frac{2i\omega}{c}\right) \hat{z} \times \mathbf{P}_t^s(\mathbf{r}_s|2\omega), \quad (7)$$

where the tangential component of the surface's nonlinear polarization is defined as

$$\mathbf{P}_t^s(\mathbf{r}_s|2\omega) = \lim_{\tau \rightarrow 0} \int_{-\tau}^{\tau} \mathbf{P}_t^{\text{NL}}(\mathbf{r}_s, z|2\omega) dz. \quad (8)$$

Equations (5) and (7) show that the tangential components of the fields are discontinuous across the interface, in contrast to the more familiar situation found in linear optics. The right-hand sides of these equations represent surface sources that can produce radiation at the second-harmonic frequency.

The components of the second-order surface susceptibility tensor  $\chi_{ijk}^s$  relate the amplitudes of the components of the nonlinear surface polarization to the fundamental field amplitudes. For the surface of an isotropic material, only three distinct components are necessary to characterize the nonlinear response of the system. These are  $\chi_{ttz}^s = \chi_{tzt}^s$ ,  $\chi_{ztt}^s$ , and  $\chi_{zzz}^s$ . The symmetry properties of the surface enable us to write

$$P_z^s(\mathbf{r}_s|2\omega) = \chi_{zzz}^s [D_z(\mathbf{r}_s|\omega)]^2 + \chi_{ztt}^s [\mathbf{E}_t(\mathbf{r}_s|\omega) \cdot \mathbf{E}_t(\mathbf{r}_s|\omega)], \quad (9)$$

$$\mathbf{P}_t^s(\mathbf{r}_s|2\omega) = \chi_{ttz}^s [\mathbf{E}_t(\mathbf{r}_s|\omega) D_z(\mathbf{r}_s|\omega)], \quad (10)$$

where we are using the convention that the permutation of the fields should yield no additional contribution to  $\mathbf{P}_t^s(\mathbf{r}_s|2\omega)$  (Ref. 30, p. 38). Notice that we have defined the surface nonlinear polarization  $\mathbf{P}^s(\mathbf{r}_s|2\omega)$  in terms of the displacement field perpendicular to the interface  $D_z(\mathbf{r}_s|\omega)$  and the tangential electric field  $\mathbf{E}_t(\mathbf{r}_s|\omega)$ , both evaluated at the surface. Inasmuch as  $\mathbf{E}_t(\mathbf{r}_s|\omega)$  and  $D_z(\mathbf{r}_s|\omega)$  are continuous across the surface, the ambiguity as to where in the selvedge the fields should be evaluated is eliminated.<sup>11</sup>

### 3. GEOMETRIES INVARIANT IN ONE DIRECTION

Some simplifications occur for systems that are invariant in one direction (in our case along  $x_2 = y$ ), illuminated perpendicularly to that direction. For the linear case it is well known that two independent sets of equations are obtained, corresponding to  $s$  and  $p$  polarization (see, e.g., Ref. 33). The problem becomes, essentially, a scalar one.

The situation for the nonlinear medium at frequency  $2\omega$  is similar. Equating to zero the partial derivatives with respect to  $x_2$  that appear in curl equations (1a) and (1b), we obtain the two independent sets:

$$\frac{\partial E_2(\mathbf{r}|2\omega)}{\partial x_3} = -i \frac{2\omega}{c} H_1(\mathbf{r}|2\omega), \quad (11a)$$

$$\frac{\partial E_2(\mathbf{r}|2\omega)}{\partial x_1} = i \frac{2\omega}{c} H_3(\mathbf{r}|2\omega), \quad (11b)$$

$$\left[ \frac{\partial H_3(\mathbf{r}|2\omega)}{\partial x_1} - \frac{\partial H_1(\mathbf{r}|2\omega)}{\partial x_3} \right] = i \frac{2\omega}{c} [\epsilon_{\text{II}}(2\omega) E_2(\mathbf{r}|2\omega) + 4\pi P_2^{\text{NL}}(\mathbf{r}|2\omega)], \quad (11c)$$

for  $s$  polarization and

$$\frac{\partial H_2(\mathbf{r}|2\omega)}{\partial x_3} = i \frac{2\omega}{c} [\epsilon_{\text{II}}(2\omega) E_1(\mathbf{r}|2\omega) + 4\pi P_1^{\text{NL}}(\mathbf{r}|2\omega)], \quad (12a)$$

$$\frac{\partial H_2(\mathbf{r}|2\omega)}{\partial x_1} = -i \frac{2\omega}{c} [\epsilon_{\text{II}}(2\omega) E_3(\mathbf{r}|2\omega) + 4\pi P_3^{\text{NL}}(\mathbf{r}|2\omega)], \quad (12b)$$

$$\left[ \frac{\partial E_3(\mathbf{r}|2\omega)}{\partial x_1} - \frac{\partial E_1(\mathbf{r}|2\omega)}{\partial x_3} \right] = -i \frac{2\omega}{c} H_2(\mathbf{r}|2\omega) \quad (12c)$$

for  $p$  polarization. The first set involves only  $H_1(\mathbf{r}|2\omega)$ ,  $H_3(\mathbf{r}|2\omega)$ ,  $E_2(\mathbf{r}|2\omega)$ , and the fundamental fields [through  $P_2^{\text{NL}}(\mathbf{r}|2\omega)$ ], whereas the second one involves only  $E_1(\mathbf{r}|2\omega)$ ,  $E_3(\mathbf{r}|2\omega)$ ,  $H_2(\mathbf{r}|2\omega)$ , and the fundamental fields [through  $P_1^{\text{NL}}(\mathbf{r}|2\omega)$  and  $P_3^{\text{NL}}(\mathbf{r}|2\omega)$ ]. So, as in the linear case, the problem is essentially of a scalar nature. In  $s$  polarization the field (either at  $\omega$  or at  $2\omega$ ) can be specified in terms of the 2-component of the electric field. Similarly, in  $p$  polarization the field is specified by the 2-component of the magnetic field. We then denote by  $\psi_{s,p}^{(\mathcal{R})}(\mathbf{r}|\Omega)$  the 2-components of the electric ( $s$  polarization) and magnetic ( $p$  polarization) fields. Here  $\mathcal{R}$  represents region I or II and  $\Omega$  stands for  $\omega$  or  $2\omega$ .

At this stage it is convenient to represent the curve that describes the profile of the surface in terms of a single parameter. We write

$$\mathbf{r}_s(t) = [\xi(t), \eta(t)], \quad (13)$$

where the vector valued function  $\mathbf{r}_s(t)$  describes the boundary as a function of parameter  $t$ . For surfaces that can be represented as single-valued functions of the  $x_1$  co-

ordinate, one can put  $\xi(t) = t = x_1$ . In such cases,  $\eta(x_1)$  represents the height of the surface as a function of  $x_1$ . For reentrant curves, such as those of interest here,  $t$  can represent the arc length along the curve<sup>34</sup> or another convenient parameter such as an angle.<sup>35</sup>

The vectors

$$\mathbf{Z} = [-\eta'(t), \xi'(t)], \quad \mathbf{X} = [\xi'(t), \eta'(t)], \quad (14)$$

of magnitude  $\phi(t) = \{[\xi'(t)]^2 + [\eta'(t)]^2\}^{1/2}$ , are normal and tangent, respectively, to the surface. The corresponding unit vectors are  $\hat{z} = \mathbf{Z}/\phi(t)$  and  $\hat{x} = \mathbf{X}/\phi(t)$ . Notice that, if parameter  $t$  is chosen as the arc length along the curve,  $\phi(t) = 1$ . Similarly, the operators of the nonnormalized normal and tangential derivatives are given by

$$\frac{\partial}{\partial Z} = \left[ -\eta'(t) \frac{\partial}{\partial x_1} + \xi'(t) \frac{\partial}{\partial x_3} \right], \quad (15a)$$

$$\frac{\partial}{\partial X} = \left[ \xi'(t) \frac{\partial}{\partial x_1} + \eta'(t) \frac{\partial}{\partial x_3} \right]. \quad (15b)$$

It should be mentioned that to evaluate the tangential derivatives on the surface it is convenient to use the relation

$$\left. \frac{\partial F(\mathbf{r})}{\partial X} \right|_{\mathbf{r}=\mathbf{r}_s} = \frac{dF(t)}{dt}, \quad (16)$$

which can be obtained by application of the chain rule.

At this stage it is also convenient to define the values of the field and its normal derivative evaluated on the surface as

$$\psi_{s,p}^{(\mathcal{R})}(t|\Omega) = \psi_{s,p}^{(\mathcal{R})}(\mathbf{r}|\Omega)|_{\mathbf{r}=\mathbf{r}_s}, \quad (17a)$$

$$Y_{s,p}^{(\mathcal{R})}(t|\Omega) = \left. \frac{\partial \psi_{s,p}^{(\mathcal{R})}(\mathbf{r}|\Omega)}{\partial Z} \right|_{\mathbf{r}=\mathbf{r}_s}. \quad (17b)$$

Let us consider first the case of  $s$  polarization. Substituting Eqs. (11a) and (11b) into (11c), we find that

$$\left[ \frac{\partial^2}{\partial x_1^2} + \frac{\partial^2}{\partial x_3^2} + \left( \frac{2\omega}{c} \right)^2 \epsilon_{\text{II}}(2\omega) \right] \psi_s^{(\text{II})}(\mathbf{r}|2\omega) = -4\pi \left( \frac{2\omega}{c} \right)^2 P_2^{\text{NL}}(\mathbf{r}|2\omega). \quad (18)$$

Thus, in the nonlinear medium, the field component  $\psi_s^{(\text{II})}(\mathbf{r}|2\omega)$  satisfies an inhomogeneous scalar two-dimensional Helmholtz equation. It is clear, however, that in medium I,  $\psi_s^{(\text{I})}(\mathbf{r}|2\omega)$  satisfies a homogeneous equation. The boundary conditions required for completion of the solution can be obtained from Eqs. (5) and (7). We find that

$$\psi_s^{(\text{I})}(t|2\omega) - \psi_s^{(\text{II})}(t|2\omega) = 0, \quad (19a)$$

$$Y_s^{(\text{I})}(t|2\omega) - Y_s^{(\text{II})}(t|2\omega) = -4\pi \left( \frac{2\omega}{c} \right)^2 \phi(t) P_y^s(t|2\omega). \quad (19b)$$

The right-hand sides of Eqs. (18) and (19b) represent the nonlinear sources.

For  $p$  polarization we follow similar steps. With the form of nonlinear polarization given by Eq. (3),  $\partial P_3^{\text{NL}}/\partial x_1 = \partial P_1^{\text{NL}}/\partial x_3$ , and we can write

$$\left[ \frac{\partial^2}{\partial x_1^2} + \frac{\partial^2}{\partial x_3^2} + \left( \frac{2\omega}{c} \right)^2 \epsilon_{\text{II}}(2\omega) \right] \psi_p^{(\text{II})}(\mathbf{r}|2\omega) = 0. \quad (20)$$

And for the boundary conditions we find that

$$\begin{aligned} \psi_p^{(\text{I})}(t|2\omega) - \psi_p^{(\text{II})}(t|2\omega) \\ = 4\pi \frac{2i\omega}{c} P_x^s(t|2\omega), \end{aligned} \quad (21a)$$

$$\begin{aligned} \frac{1}{\epsilon_{\text{I}}(2\omega)} Y_p^{(\text{I})}(t|2\omega) - \frac{1}{\epsilon_{\text{II}}(2\omega)} Y_p^{(\text{II})}(t|2\omega) \\ = -4\pi \frac{2i\omega}{c} \left[ \frac{dP_z^s(t|2\omega)}{dt} + \frac{\phi(t)P_x^{\text{NL}}(t|2\omega)}{\epsilon_{\text{II}}(2\omega)} \right]. \end{aligned} \quad (21b)$$

Equation (20) shows that the bulk contribution to the second-harmonic field vanishes, whereas Eqs. (21) contain nonzero contributions from the surface. It is worth pointing out, however, that the second term on the right-hand side of Eq. (21b) is in fact a mixed term; it represents the bulk nonlinear polarization evaluated on the surface.

From Eqs. (3) and (10), the sources of the  $s$ -polarized second-harmonic field that appear on the right-hand sides of Eqs. (18) and (19b) can be written in the form

$$\begin{aligned} P_2^{\text{NL}}(\mathbf{r}|2\omega) = \alpha \frac{ic}{\omega \epsilon_{\text{II}}(\omega)} \left[ \frac{\partial \psi_p^{(\text{II})}(\mathbf{r}|\omega)}{\partial x_1} \frac{\partial \psi_s^{(\text{II})}(\mathbf{r}|\omega)}{\partial x_3} \right. \\ \left. - \frac{\partial \psi_p^{(\text{II})}(\mathbf{r}|\omega)}{\partial x_3} \frac{\partial \psi_s^{(\text{II})}(\mathbf{r}|\omega)}{\partial x_1} \right], \end{aligned} \quad (22a)$$

$$\phi(t)P_y^s(t|2\omega) = -\chi_{titz}^s \left( \frac{c}{i\omega} \right) \psi_s^{(\text{I})}(t|\omega) \frac{d\psi_p^{(\text{I})}(t|\omega)}{dt}. \quad (22b)$$

It is interesting to note that, if the excitation field is purely  $s$  or  $p$  polarized, both of these sources vanish, and there is no  $s$ -polarized second-harmonic radiation.

From Eqs. (3), (9), and (10) the sources of the  $p$ -polarized second-harmonic field can be written as

$$\begin{aligned} \phi(t)P_x^{\text{NL}}(t|2\omega) = -(\alpha/2 + \gamma) \frac{c^2}{\omega^2} \left\{ \frac{1}{\epsilon_{\text{I}}^2(\omega)} \frac{d}{dt} \left[ \frac{Y_p^{(\text{I})}(t|\omega)}{\phi(t)} \right]^2 \right. \\ \left. + \frac{1}{\epsilon_{\text{II}}^2(\omega)} \frac{d}{dt} \left[ \frac{1}{\phi(t)} \frac{d\psi_p^{(\text{I})}(t|\omega)}{dt} \right]^2 \right\} \\ - \frac{\alpha}{2\epsilon_{\text{II}}(\omega)} \frac{d}{dt} [\psi_p^{(\text{I})}(t|\omega)]^2 \\ + \gamma \frac{d}{dt} [\psi_s^{(\text{I})}(t|\omega)]^2, \end{aligned} \quad (23a)$$

$$P_x^s(t|2\omega) = \frac{\chi_{titz}^s}{\epsilon_{\text{I}}(\omega)} \left( \frac{c}{\omega} \right)^2 \frac{1}{\phi^2(t)} Y_p^{(\text{I})}(t|\omega) \frac{d\psi_p^{(\text{I})}(t|\omega)}{dt}, \quad (23b)$$

$$\begin{aligned} P_z^s(t|2\omega) = -\chi_{zzz}^s \left( \frac{c}{\omega} \right)^2 \left[ \frac{1}{\phi(t)} \frac{d\psi_p^{(\text{I})}(t|\omega)}{dt} \right]^2 \\ - \chi_{ztt}^s \left\{ \frac{1}{\epsilon_{\text{I}}^2(\omega)} \left( \frac{c}{\omega} \right)^2 \left[ \frac{Y_p^{(\text{I})}(t|\omega)}{\phi(t)} \right]^2 \right. \\ \left. - [\psi_s^{(\text{I})}(t|\omega)]^2 \right\}. \end{aligned} \quad (23c)$$

#### 4. INTEGRAL EQUATION METHOD

Application of Green's second integral theorem to region I yields the total field in this region in terms of the boundary values of the field and its normal derivative.<sup>36</sup> We can write

$$\begin{aligned} \psi_{s,p}^{(\text{I})}(\mathbf{r}|\Omega) = \psi_{s,p}^{(\text{I})}(\mathbf{r}|\Omega)_{\text{inc}} + \frac{1}{4\pi} \int_{\Gamma} \left\{ \frac{\partial G_{\Omega}^{\text{I}}(\mathbf{r}|\mathbf{r}')}{\partial Z'} \right\}_{\mathbf{r}'=\mathbf{r}_s(t')} \\ \times \psi_{s,p}^{(\text{I})}(t'|\Omega) - G_{\Omega}^{\text{I}}[\mathbf{r}|\mathbf{r}_s(t')] Y_{s,p}^{(\text{I})}(t'|\Omega) \Big\} dt', \end{aligned} \quad (24)$$

where we have used the fact that the element of arc of  $\Gamma$  is  $ds = \phi(t)dt$ .

In this expression  $\psi_{s,p}^{(\text{I})}(\mathbf{r}|\Omega)_{\text{inc}}$  represents the incident field,  $\psi_{s,p}^{(\text{I})}(\mathbf{r}|2\omega)_{\text{inc}} = 0$ , and Green's function  $G_{\Omega}^{\text{I}}(\mathbf{r}|\mathbf{r}')$  for region I may be expressed in terms of a Hankel function of the first kind:

$$G_{\Omega}^{\text{I}}(\mathbf{r}|\mathbf{r}') = i\pi H_0^{(1)} \left[ n_{\text{I}}(\Omega) \frac{\Omega}{c} |\mathbf{r} - \mathbf{r}'| \right], \quad (25)$$

where  $n_{\text{I}}(\Omega)$  is the refractive index of medium I. The scattered field is given by the second term on the right-hand side of Eq. (24) and can be calculated if the source functions  $\psi_{s,p}^{(\text{I})}(t|\Omega)$  and  $Y_{s,p}^{(\text{I})}(t|\Omega)$  are known.

By letting the point of observation approach the surface in Eq. (24), and following a similar procedure with a second equation obtained by the application of Green's theorem to medium II, we can derive the following two equations<sup>36</sup>:

$$\begin{aligned} \psi_{s,p}^{(\text{I})}(t|\Omega) = \psi_{s,p}^{(\text{I})}(t|\Omega)_{\text{inc}} \\ + \frac{1}{4\pi} \lim_{\tau \rightarrow 0} \int_{\Gamma} \left\{ \frac{\partial G_{\Omega}^{\text{I}}(\mathbf{r}_s^+|\mathbf{r}')}{\partial Z'} \right\}_{\mathbf{r}'=\mathbf{r}_s(t')} \psi_{s,p}^{(\text{I})}(t'|\Omega) \\ - G_{\Omega}^{\text{I}}[\mathbf{r}_s^+|\mathbf{r}_s(t')] Y_{s,p}^{(\text{I})}(t'|\Omega) \Big\} dt', \end{aligned} \quad (26a)$$

$$\begin{aligned} 0 = -\frac{1}{4\pi} \lim_{\tau \rightarrow 0} \int_{\Gamma} \left\{ \frac{\partial G_{\Omega}^{\text{II}}(\mathbf{r}_s^+|\mathbf{r}')}{\partial Z'} \right\}_{\mathbf{r}'=\mathbf{r}_s(t')} \psi_{s,p}^{(\text{II})}(t'|\Omega) \\ - G_{\Omega}^{\text{II}}[\mathbf{r}_s^+|\mathbf{r}_s(t')] Y_{s,p}^{(\text{II})}(t'|\Omega) \Big\} dt' \\ - \frac{1}{4\pi} \int_{S_B} G_{\Omega}^{\text{II}}(\mathbf{r}_s^+|\mathbf{r}'_B) F_{s,p}^{\text{NL}}(\mathbf{r}'_B|\Omega) dS'_B, \end{aligned} \quad (26b)$$

where  $\mathbf{r}_s^+ = \mathbf{r}_s(t) + \tau \hat{z}$ ,  $G_\Omega^{\text{II}}(\mathbf{r}|\mathbf{r}')$  is Green's function of medium II, and the boundary values  $\psi_{s,p}^{(\text{II})}(t|\Omega)$  and  $Y_{s,p}^{(\text{II})}(t|\Omega)$  correspond to fields in medium II. The integral over region  $S_B$  in Eq. (26b) represents the nonlinear bulk contribution of the material. Evidently,  $F_{s,p}^{\text{NL}}(\mathbf{r}_B|\omega) = 0$ , whereas  $F_s^{\text{NL}}(\mathbf{r}_B|2\omega) = -4\pi(2\omega/c)^2 P_2^{\text{NL}}(\mathbf{r}_B|2\omega)$  for  $s$  polarization and  $F_p^{\text{NL}}(\mathbf{r}_B|2\omega) = 0$  for  $p$  polarization, according to Eqs. (18) and (20), respectively. By similarity to the description of the boundary profile it is convenient

$$0 = \sum_{n=1}^N \left[ H_{mn}^{\text{II}}(\omega) \psi_{s,p}^{(\text{I})}(t_n|\omega) - \frac{\nu_{\text{II}}(\omega)}{\nu_{\text{I}}(\omega)} L_{mn}^{\text{II}}(\omega) Y_{s,p}^{(\text{I})}(t_n|\omega) \right], \quad (29b)$$

where the matrix elements  $H_{mn}^{\text{I}}(\omega)$  and  $L_{mn}^{\text{I}}(\omega)$  are given by

$$H_{mn}^{\text{I}}(\omega) = \begin{cases} \frac{i\Delta t_n}{4} n_{\text{I}}(\omega) \frac{\omega}{c} [-\eta'_n(\xi_m - \xi_n) + \xi'_n(\eta_m - \eta_n)] \frac{H_1^{(\text{I})}\{n_{\text{I}}(\omega)(\omega/c)[(\xi_m - \xi_n)^2 + (\eta_m - \eta_n)^2]^{1/2}\}}{[(\xi_m - \xi_n)^2 + (\eta_m - \eta_n)^2]^{1/2}} & m \neq n \\ \frac{1}{2} + \frac{\Delta t_m}{4\pi\phi^2(t_m)} (\xi'_m \eta''_m - \xi''_m \eta'_m) & m = n \end{cases}, \quad (30a)$$

$$L_{mn}^{\text{I}}(\omega) = \begin{cases} \frac{i\Delta t_n}{4} H_0^{(\text{I})} \left\{ n_{\text{I}}(\omega) \frac{\omega}{c} [(\xi_m - \xi_n)^2 + (\eta_m - \eta_n)^2]^{1/2} \right\} & m \neq n \\ \frac{i\Delta t_m}{4} H_0^{(\text{I})} \left[ \frac{\Delta t_m n_{\text{I}}(\omega)(\omega/c)\phi(t_m)}{2e} \right], & m = n \end{cases}, \quad (30b)$$

to write  $\mathbf{r}_B$  in terms of two parameters,  $\tau_1$  and  $\tau_2$ , through the functions  $\xi_B$  and  $\eta_B$ , as

$$\mathbf{r}_B(\tau_1, \tau_2) = [\xi_B(\tau_1, \tau_2), \eta_B(\tau_1, \tau_2)]. \quad (27)$$

Equations (26) can be coupled, leading to a system of two equations with two unknowns. In the linear case the coupling is through the conditions of continuity for the tangential components of the field, and, in the second-harmonic case, through Eqs. (19) and (21). We then can write

$$\psi_{s,p}^{(\text{I})}(t|\Omega) - \psi_{s,p}^{(\text{II})}(t|\Omega) = A_{s,p}(t|\Omega), \quad (28a)$$

$$\frac{1}{\nu_{\text{I}}(\Omega)} Y_{s,p}^{(\text{I})}(t|\Omega) - \frac{1}{\nu_{\text{II}}(\Omega)} Y_{s,p}^{(\text{II})}(t|\Omega) = B_{s,p}(t|\Omega), \quad (28b)$$

where  $\nu_{\text{I,II}}(\Omega) = \epsilon_{\text{I,II}}(\Omega)$  in  $p$  polarization and  $\nu_{\text{I,II}}(\Omega) = 1$  in  $s$  polarization. It is clear that  $A_{s,p}(t|\omega) = B_{s,p}(t|\omega) = 0$ .  $A_s(t|2\omega)$  and  $A_p(t|2\omega)$ , however, are given by the right-hand sides of (19a) and (21a), respectively, and  $B_s(t|2\omega)$  and  $B_p(t|2\omega)$  are given by the right-hand sides of Eqs. (19b) and (21b); the nonlinear sources are given by Eqs. (22) and (23).

In the discretization procedure we take a set of  $N$  elements, i.e.,  $[t_1, \dots, t_n]$ , which allows us to write the following matrix equations for the linear case:

$$\psi_{s,p}^{(\text{I})}(t_m|\omega) = \psi_{s,p}^{(\text{I})}(t_m|\omega)_{\text{inc}} + \sum_{n=1}^N [H_{mn}^{\text{I}}(\omega) \psi_{s,p}^{(\text{I})}(t_n|\omega) - L_{mn}^{\text{I}}(\omega) Y_{s,p}^{(\text{I})}(t_n|\omega)], \quad (29a)$$

where  $\Delta t_n = t_n - t_{n-1}$  is the length of the sampling intervals and we are using the notation  $\xi_n = \xi(t_n)$ ,  $\xi'_n = \xi'(t_n)$ ,  $\xi''_n = \xi''(t_n)$ ,  $\eta_n = \eta(t_n)$ ,  $\eta'_n = \eta'(t_n)$ , and  $\eta''_n = \eta''(t_n)$ . These expressions reduce to those given in Ref. 34 when the parameter  $t$  is taken as the arc length along the curve. We obtain matrix elements  $H_{mn}^{\text{II}}(\omega)$  and  $L_{mn}^{\text{II}}(\omega)$  by replacing  $n_{\text{I}}(\omega)$  with  $n_{\text{II}}(\omega)$  in Eqs. (30).

Similarly, for the second-harmonic fields we find that

$$\psi_{s,p}^{(\text{I})}(t_m|2\omega) = \sum_{n=1}^N [H_{mn}^{\text{I}}(2\omega) \psi_{s,p}^{(\text{I})}(t_n|2\omega) - L_{mn}^{\text{I}}(2\omega) Y_{s,p}^{(\text{I})}(t_n|2\omega)], \quad (31a)$$

$$\mathcal{Q}_{s,p}(t_m|2\omega) = \sum_{n=1}^N \left[ H_{mn}^{\text{II}}(2\omega) \psi_{s,p}^{(\text{I})}(t_n|2\omega) - \frac{\nu_{\text{II}}(2\omega)}{\nu_{\text{I}}(2\omega)} L_{mn}^{\text{II}}(2\omega) Y_{s,p}^{(\text{I})}(t_n|2\omega) \right], \quad (31b)$$

where

$$\begin{aligned} \mathcal{Q}_{s,p}(t_m|2\omega) = & \sum_{n=1}^N [H_{mn}^{\text{II}}(2\omega) A_{s,p}(t_n|2\omega) \\ & - \nu_{\text{II}}(2\omega) L_{mn}^{\text{II}}(2\omega) B_{s,p}(t_n|2\omega)] \\ & + \sum_{l=1}^{N_1} \sum_{j=1}^{N_2} \mathcal{L}_{mlj}^{\text{II}}(2\omega) F_{s,p}^{\text{NL}}(\tau_{1l}, \tau_{2j}|2\omega) \\ & \times \phi_1(\tau_{1l}, \tau_{2j}) \phi_2(\tau_{1l}, \tau_{2j}). \end{aligned} \quad (32)$$

In writing the second term on the right-hand of Eq. (32) we sampled the bulk region in pairs  $(\tau_{1l}, \tau_{2j})$  with  $l = 1, \dots, N_1$  and  $j = 1, \dots, N_2$ . The functions  $\phi_1$  and  $\phi_2$  can be written as

$$\phi_1(\tau_{1l}, \tau_{2j}) = \left\{ \left[ \frac{\partial \xi_B}{\partial \tau_1}(\tau_{1l}, \tau_{2j}) \right]^2 + \left[ \frac{\partial \eta_B}{\partial \tau_1}(\tau_{1l}, \tau_{2j}) \right]^2 \right\}^{1/2},$$

$$\phi_2(\tau_{1l}, \tau_{2j}) = \left\{ \left[ \frac{\partial \xi_B}{\partial \tau_2}(\tau_{1l}, \tau_{2j}) \right]^2 + \left[ \frac{\partial \eta_B}{\partial \tau_2}(\tau_{1l}, \tau_{2j}) \right]^2 \right\}^{1/2}.$$

Matrix elements  $H_{mn}^{I,II}(2\omega)$  and  $L_{mn}^{I,II}(2\omega)$  are the same as elements  $H_{mn}^{I,II}(\omega)$  and  $L_{mn}^{I,II}(\omega)$  but are evaluated at  $2\omega$ , and matrix elements  $\mathcal{L}_{mlj}^{II}(2\omega)$  are given by

$$\begin{aligned} \mathcal{L}_{mlj}^{II}(2\omega) &= \frac{i\Delta\tau_{1l}\Delta\tau_{2j}}{4} H_0^{(1)} \left( n_{II}(2\omega) \frac{2\omega}{c} \right. \\ &\quad \times \{ [\xi_m - \xi_B(\tau_{1l}, \tau_{2j})]^2 \\ &\quad \left. + [\eta_m - \eta_B(\tau_{1l}, \tau_{2j})]^2 \}^{1/2} \right), \end{aligned} \quad (33)$$

where  $\Delta\tau_{1l} = \tau_{1l} - \tau_{1(l-1)}$  and  $\Delta\tau_{2j} = \tau_{2j} - \tau_{2(j-1)}$  are the lengths of the sampling intervals in the volume. From the form of matrix equations (31) it is clear that the function  $\mathcal{Q}_{s,p}(t_m|2\omega)$  constitutes the source that produces the harmonic field. With the solution of the linear problem, the functions  $A_{s,p}(t_n|2\omega)$  and  $B_{s,p}(t_n|2\omega)$  can be calculated. These, in turn, are used for the determination of the nonlinear source functions  $\psi_{s,p}^{(I)}(t_n|2\omega)$  and  $Y_{s,p}^{(I)}(t_n|2\omega)$ , which are required for the calculation of the scattered field at  $2\omega$ .

With reference to the geometry shown in Fig. 2, the field scattered by the particle into medium I may be written as

$$\begin{aligned} \psi_{s,p}^{(I)}(r, \theta|\Omega)_{sc} &= \frac{i}{4} \int_{\Gamma} \left\{ (\mathbf{Z}' \cdot \hat{\mathbf{u}}) n_I(\Omega) \frac{\Omega}{c} \right. \\ &\quad \times H_1^{(1)} \left[ n_I(\Omega) \frac{\Omega}{c} |\mathbf{u}| \right] \psi_{s,p}^{(I)}(t'|\Omega) \\ &\quad \left. - H_0^{(1)} \left[ n_I(\Omega) \frac{\Omega}{c} |\mathbf{u}| \right] Y_{s,p}^{(I)}(t'|\Omega) \right\} dt', \end{aligned} \quad (34)$$

where  $(r, \theta)$  represent the coordinates of the point of observation,  $\mathbf{u} = [r \cos \theta - \xi(t')]\hat{\mathbf{x}}_1 + [r \sin \theta - \eta(t')]\hat{\mathbf{x}}_3$ , and  $\hat{\mathbf{u}}$  is a unit vector in the direction of  $\mathbf{u}$ . For large values of  $r$  we have

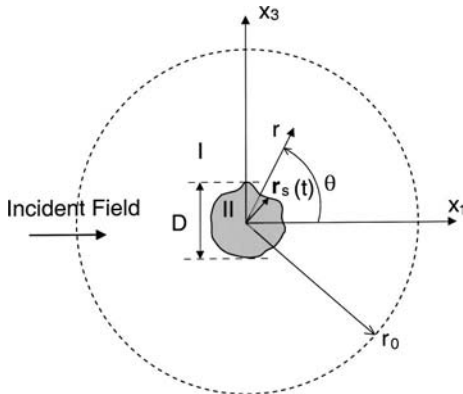


Fig. 2. Schematic diagram of the scattering geometry.

$$\begin{aligned} \psi_{s,p}^{(I)}(r, \theta|\Omega)_{sc} \\ = \exp[i(\pi/4)] \frac{\exp[in_I(\Omega)(\Omega/c)r]}{[8\pi n_I(\Omega)(\Omega/c)r]^{1/2}} S_{s,p}(\theta|\Omega), \end{aligned} \quad (35)$$

where the scattering amplitude

$$\begin{aligned} S_{s,p}(\theta|\Omega) &= \int_{\Gamma} \left\{ in_I(\Omega) \frac{\Omega}{c} [\eta'(t') \cos \theta - \xi'(t') \sin \theta] \right. \\ &\quad \times \left. \psi_{s,p}^{(I)}(t'|\Omega) - Y_{s,p}^{(I)}(t'|\Omega) \right\} \\ &\quad \times \exp \left\{ -in_I(\Omega) \frac{\Omega}{c} [\xi(t') \cos \theta \right. \\ &\quad \left. + \eta(t') \sin \theta] \right\} dt'. \end{aligned} \quad (36)$$

In writing Eqs. (35) and (36) we used the expansion of Hankel functions for large arguments<sup>37</sup> and the approximation  $|\mathbf{u}| \approx r - [\xi(t)\cos\theta + \eta(t)\sin\theta]$  for the argument of the exponential.

We can evaluate the total power scattered by a two-dimensional particle by constructing an imaginary cylinder of length  $L$  and radius  $r_0$  that encloses the particle (Fig. 2). The scattered power crossing this imaginary surface can be written as

$$P(\Omega)_{sc} = r_0 L \int_0^{2\pi} \mathbf{S}_{sc}(r_0, \theta|\Omega) \cdot \hat{\mathbf{e}}_r d\theta, \quad (37)$$

where

$$\mathbf{S}_{sc}(r_0, \theta|\Omega) = (c/8\pi) \Re[\mathbf{E}_{sc}(r_0, \theta|\Omega) \cdot \mathbf{H}_{sc}^*(r_0, \theta|\Omega)]$$

is the time average of the Poynting vector of the scattered fields. It is straightforward to show that

$$\begin{aligned} P_{s,p}(\Omega)_{sc} &= \frac{r_0 L c}{8\pi \nu_I(\Omega)(\Omega/c)} \Re \left\{ i \int_0^{2\pi} \psi_{s,p}^{(I)}(r_0, \theta|\Omega)_{sc} \right. \\ &\quad \times \left. \left[ \frac{\partial \psi_{s,p}^{(I)}(r_0, \theta|\Omega)_{sc}}{\partial r} \right]^* d\theta \right\} \\ &= \frac{Lc}{64\pi^2 \nu_I(\Omega)(\Omega/c)} \int_0^{2\pi} |S_{s,p}(\theta|\Omega)|^2 d\theta. \end{aligned} \quad (38)$$

We write the incident power  $P(\omega)_{inc}$  intersecting a particle of cross section  $\sigma = DL$  (Fig. 2) as the sum of the contributions from the two field components:

$$P_s(\omega)_{inc} = \sigma n_I(\omega) \frac{c}{8\pi} |\psi_{0s}|^2, \quad (39a)$$

$$P_p(\omega)_{inc} = \sigma \frac{1}{n_I(\omega)} \frac{c}{8\pi} |\psi_{0p}|^2, \quad (39b)$$

where  $\psi_{0s}$  and  $\psi_{0p}$  are the amplitudes of the incident wave components  $E_2$  and  $H_2$ . At the fundamental frequency there are no changes in the polarization, and the scattering cross-section of the particle can be expressed as

$$Q_{\zeta}(\omega) = \frac{P_{\zeta}(\omega)_{sc}}{P_{\zeta}(\omega)_{inc}} = \int_0^{2\pi} q_{\zeta}(\theta|\omega) d\theta, \quad (40)$$

where  $s$  represents either  $s$  or  $p$  and the differential scattering cross section is given by

$$q_s(\theta|\omega) = \frac{1}{8\pi D(\omega/c)} \frac{1}{n_1(\omega)} \frac{|S_s(\theta|\omega)|^2}{|\psi_{0s}|^2}. \quad (41)$$

At the harmonic frequency there can be polarization changes, but, as we have seen, when the particle is illuminated with pure  $s$  or  $p$  polarization the second-harmonic radiation is always  $p$  polarized. To get second-harmonic radiation in  $s$  polarization it is necessary to illuminate the particle with mixed polarization. Inasmuch as, in the calculations, only pure  $s$ - or  $p$ -polarized illumination is considered, we simplify the notation by assuming such situations. Then the scattering cross section at  $2\omega$  can be defined as

$$Q_{ps}(2\omega) = \sigma \frac{P_p(2\omega)_{sc}}{[P_s(\omega)_{inc}]^2} = \int_0^{2\pi} q_{ps}(\theta|2\omega) d\theta, \quad (42)$$

where the differential scattering cross section for the second-harmonic radiation is given by

$$q_{ps}(\theta|2\omega) = \frac{1}{2\omega D} \left[ \frac{\nu_1^2(\omega)}{n_1^2(\omega)\nu_1(2\omega)} \right] \frac{|S_p(\theta|2\omega)|^2}{|\psi_{0s}|^4}. \quad (43)$$

In common with most studies of planar and rough surfaces, our results for the second-harmonic scattering cross-section and the second-harmonic differential scattering cross section are expressed in units of  $\text{cm}^2/W$  and  $\text{cm}^2/W \text{ rad}$ , respectively.

## 5. RESULTS AND DISCUSSION

In this section we illustrate our theoretical results through calculation of the scattering cross section and the differential scattering cross section (angular intensity distribution) for particles of various shapes at frequencies  $\omega$  and  $2\omega$ . We consider particles of a free-electron medium, taking for the dielectric function as a function of frequency a best fit of the free-electron model to experimental data for silver.<sup>38</sup> For consistency, the nonlinear susceptibilities employed are calculated with a free-electron model for the nonlinear polarization. The model is relatively simple and leads to analytical expressions for the nonlinear susceptibilities. These assumptions would appear realistic for modeling silver particles in the infrared.

In the free-electron model, the nonlinear polarization takes the form given by Eq. (3), with<sup>29</sup>

$$\alpha = 0, \quad \beta = \frac{e}{8\pi m_0 \omega^2}, \quad \gamma = \frac{e^3 n_0(z)}{8m_0^2 \omega^4}.$$

Here,  $e$  and  $m_0$  are the electron charge and mass, respectively, and  $n_0(z)$  is the position-dependent electron number density. For points above the interface,  $n_0(z) = 0$  and  $\epsilon_{II}(\omega) = 1$ . Inside the medium, however,  $n_0(z) = n_B$ ,  $\epsilon_{II}(\omega) = 1 - \omega_p^2/\omega^2$ , where  $\omega_p = (4\pi e^2 n_B/m)^{1/2}$  is the plasma frequency and  $n_B$  is the bulk electron number density. It then follows that we can write  $\gamma = (\beta/4) \times [1 - \epsilon_{II}(\omega)]$ .

The integrals of  $P_z^{\text{NL}}$  and  $\mathbf{P}_t^{\text{NL}}$  across the interface determine the surface polarizations [Eqs. (6) and (8)]. In

the limit  $\tau \rightarrow 0$ , only the singular parts of the tangential and normal components of the nonlinear polarization provide a contribution to the second-harmonic field. The unbounded terms are<sup>29</sup>

$$\mathbf{P}_t^{\text{NL}}(x, z|2\omega) \approx \beta \mathbf{E}_t(x, z|\omega) \frac{\partial \mathbf{E}_z(x, z|\omega)}{\partial z}, \quad (44)$$

$$P_z^{\text{NL}}(x, z|2\omega) \approx \gamma \frac{\partial E_z^2(x, z|\omega)}{\partial z} + \beta E_z(x, z|\omega) \frac{\partial E_z(x, z|\omega)}{\partial z}. \quad (45)$$

From Eqs. (6) and (9), and (8) and (10), we find that

$$\chi_{zzz}^s = -\frac{2}{3} \beta \left\{ \frac{[\epsilon_{II}(\omega) - 1][\epsilon_{II}(\omega) - 3]}{2\epsilon_{II}^2(\omega)} - \frac{2}{3} \ln \left[ \frac{\epsilon_{II}(\omega)}{\epsilon_{II}(2\omega)} \right] \right\}, \quad (46a)$$

$$\chi_{ztt}^s = 0, \quad (46b)$$

$$\chi_{ttz}^s = \beta \left[ \frac{\epsilon_{II}(\omega) - 1}{\epsilon_{II}(\omega)} \right]. \quad (46c)$$

In the examples presented we consider that the system is illuminated by an  $s$ - or a  $p$ -polarized plane wave traveling in the  $+x_1$  direction (Fig. 2). The kinds of particle studied are illustrated in Fig. 3. The simplest case is the particle with circular cross section depicted in Fig. 3(a) (i.e., a cylinder). We also consider particles with elliptical cross sections and general orientations, as illustrated in Fig. 3(b), and sinusoidally modulated particles of the type shown in Fig. 3(c). The shapes illustrated in Figs. 3(b) and 3(c) can be viewed as perturbations of the cylindrical shape of Fig. 3(a).

In Figs. 4 and 5 we present calculations of the scattering efficiency of a cylinder as a function of the parameter  $(\Omega/c)R$  for both fundamental and harmonic light by keeping the radius fixed at  $R = 0.5 \mu\text{m}$  and varying the incident wavelength in the range  $0.140$ – $1.26 \mu\text{m}$ . Figure 4(a) contains the results of the linear calculations for incident  $p$  polarization. The solid curve corresponds to the analytical Mie-type calculations,<sup>32</sup> and the dotted curve represent calculations with the numerical technique described in this paper. The results for second-harmonic efficiency are shown in Fig. 4(b). The corresponding results for illumination with  $s$ -polarized light are shown in Fig. 5. One can observe very good agreement between the results obtained with the two theoretical methods, showing the consistency between them.

For illumination with  $p$  polarization, the efficiency at the fundamental frequency presents an oscillatory behavior in the region  $8 \leq \omega R/c \leq 13$  [Fig. 4(a)]. Well-defined peaks are observed at specific values of the frequency, which denote the presence of morphology-dependent resonances.<sup>39</sup> In this region of relatively high efficiency the linear and, thus, the nonlinear sources are expected to be large. The resonant behavior should then be reflected in the efficiency of SHG, as is indeed we observe in the region  $23 \leq 2\omega R/c \leq 27$  of Fig. 4(b), where we find oscillations whose maxima coincide with the peaks in the curve for the linear efficiency. Other interesting features are found in the region  $8 \leq 2\omega R/c \leq 13$ , which corre-

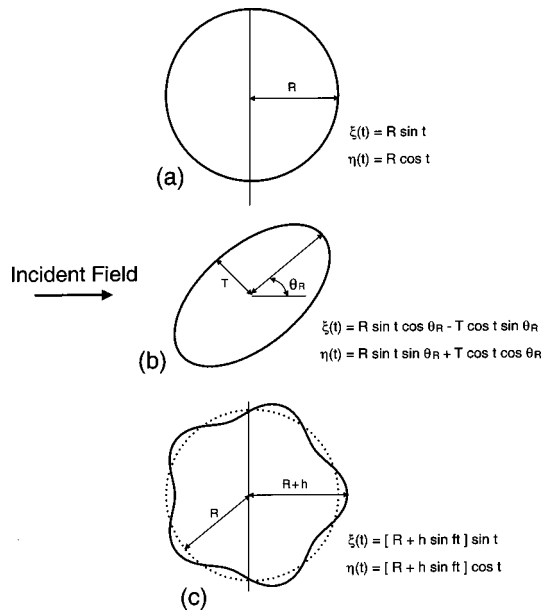


Fig. 3. Illustration of the three kinds of particle considered in the calculations: particles with (a) circular geometrical cross section, (b) elliptical geometrical cross section, and (c) sinusoidally perturbed geometrical cross section.

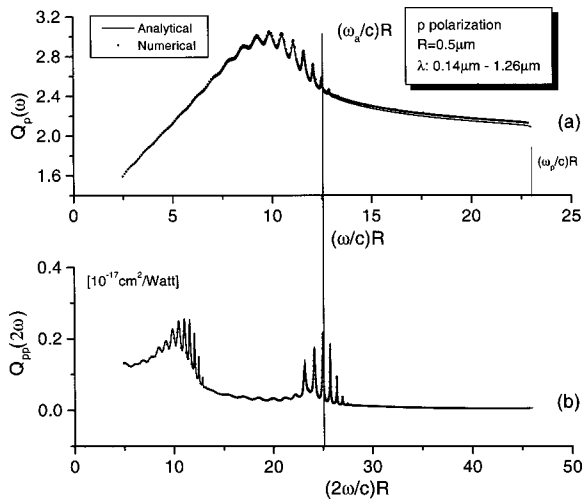


Fig. 4. Scattering cross section for a cylinder illuminated with  $p$ -polarized light. (a) Fundamental frequency, (b) second-harmonic frequency.  $R$  is the radius of the cylinder.

sponds roughly to the same ratio  $R/\lambda$  that led to the shape resonances of the linear efficiency of Fig. 4(a).

With  $s$ -polarized illumination, the behavior of the linear efficiency curve is flat, denoting the absence of well-defined resonances [Fig. 5(a)]. Interestingly, however, at the harmonic frequency the light is  $p$  polarized, and the excitation of resonances is clearly visible in the region  $23 \leq 2\omega R/c \leq 27$  [Fig. 5(b)]. The shape resonances that are present in the region  $8 \leq 2\omega R/c \leq 13$  are barely excited in this case. Another noteworthy fact is that the second-harmonic efficiency for this case of  $s$ -polarized illumination is 2 orders of magnitude below the second-harmonic efficiency for  $p$ -polarized illumination.

The differential scattering cross sections for illumination with  $p$ - and  $s$ -polarized light of wavelengths  $\lambda = 0.250 \mu\text{m}$  and  $\lambda = 0.570 \mu\text{m}$  are shown in Figs. 6 and

7, respectively. The chosen wavelengths correspond to the positions denoted by vertical lines in Figs. 4 and 5. In the linear calculations a sharp forward-scattering lobe can be observed in both cases, with a small, fairly isotropic contribution. The forward lobe is much sharper in the  $p$ -polarized case. The two second-harmonic distributions, however, have radically different shapes. The curve that corresponds to incident  $p$ -polarized light is 4 orders of magnitude greater the other curve and is based toward backscattering angles. We observe from the figure that the agreement between the numerical results and those based on analytical expressions is excellent. It is also worth pointing out that at the exact forward-scattering and backscattering angles the second-harmonic differential scattering cross sections appear to be zero. As we argue below, the differential scattering cross section is exactly zero in these directions, which represents a general result for systems with symmetry about the  $x_1$  axis.

Consider a situation in which both the particle and the illumination are symmetric about axis  $x_1$ . The fact that there is no harmonic radiation along this axis can be inferred from the form of the nonlinear sources that appear on the right-hand sides of Eqs. (18) and (19) for the generation of  $s$ -polarized light and on the right hand sides of Eqs. (20) and (21) for  $p$ -polarized light. The corresponding expressions for these nonlinear sources in terms of the fundamental source functions are given by Eqs. (22) for  $s$  polarization and by Eqs. (23) for  $p$  polarization. First it should be noted that for a symmetrical particle the linear source functions  $\psi_{s,p}^{(1)}(t|\omega)$  and  $P_{s,p}^{(1)}(t|\omega)$ , as well as the field inside the particle, must be symmetrical about axis  $x_1$ . Derivatives with respect to  $x_3$  and with respect to  $t$  are, thus, antisymmetric. On inspecting Eqs. (22) and (23) we conclude that all the nonlinear source functions are antisymmetric. This implies that the total second-harmonic radiation along  $x_1$  should be zero, explaining the lack of second-harmonic radiation along the optical axis observed in Figs. 6(b) and 7(b).

It is also of interest to compare the efficiencies produced by particles with different geometries. In Fig. 8

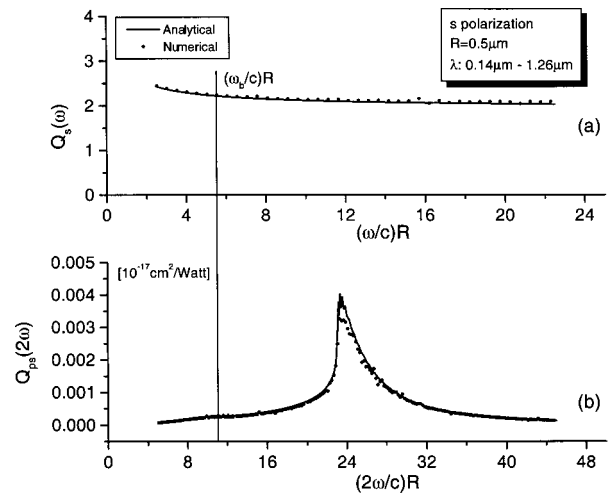


Fig. 5. Scattering cross section for a cylinder illuminated with  $s$ -polarized light. (a) Fundamental frequency, (b) second-harmonic frequency.  $R$  is the radius of the cylinder.

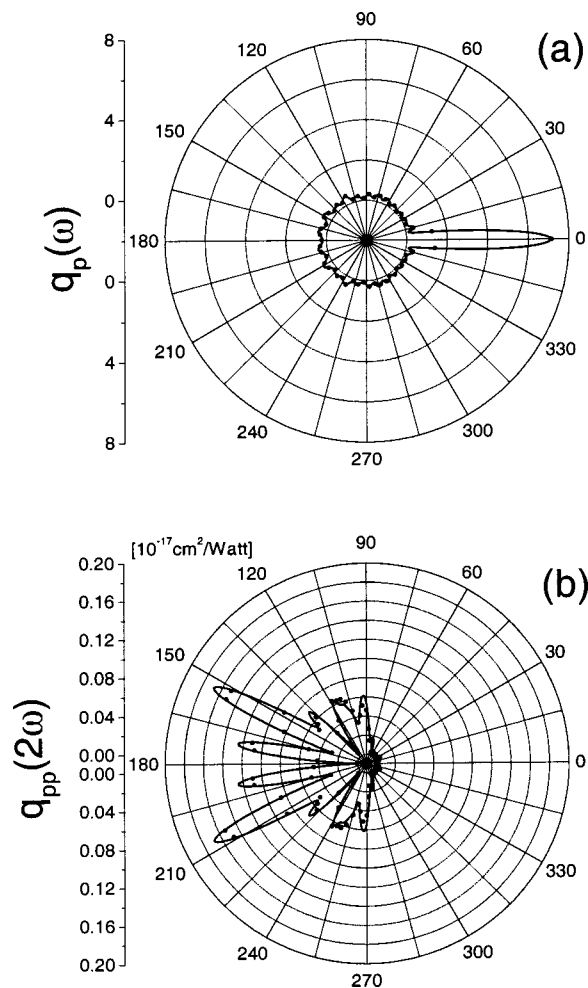


Fig. 6. Differential scattering cross sections for a cylinder illuminated with  $p$ -polarized light of wavelength  $\lambda = 0.25 \mu\text{m}$ . (a) Fundamental frequency, (b) second-harmonic frequency. The analytical results are shown with solid curves and the numerical results are shown with filled circles. The radius of the cylinder is  $0.5 \mu\text{m}$ .

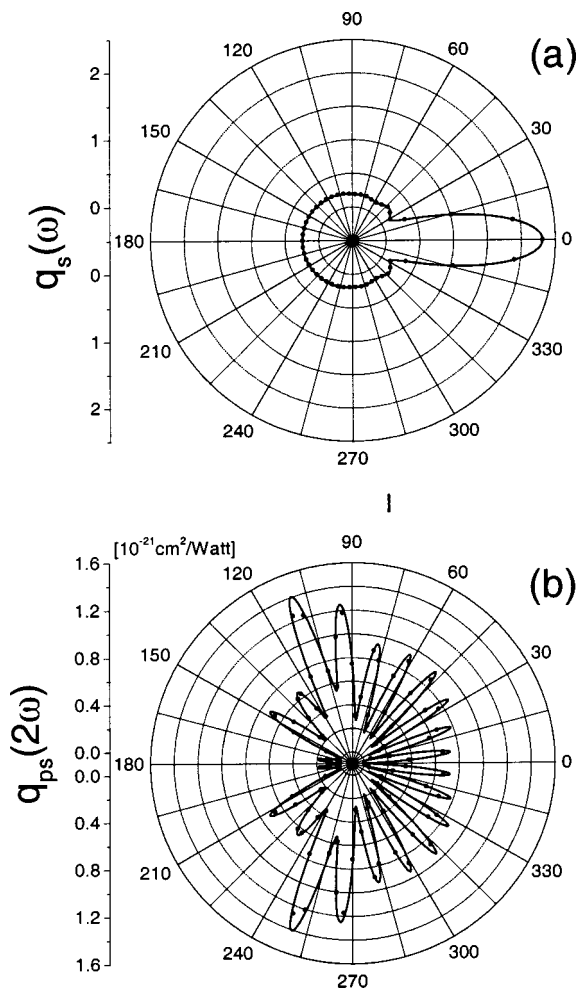


Fig. 7. Differential scattering cross sections for a cylinder illuminated with  $s$ -polarized light of wavelength  $\lambda = 0.57 \mu\text{m}$ . (a) Fundamental frequency, (b) second-harmonic frequency. The analytical results are shown with solid curves, and the numerical results are shown with filled circles. The radius of the cylinder is  $0.5 \mu\text{m}$ .

we present results for the scattering cross sections of particles with circular, elliptical, and sinusoidally perturbed cross sections, illuminated with  $p$ -polarized light in the range  $\lambda = 0.24\text{--}0.31 \mu\text{m}$ . In all cases  $R = 0.5 \mu\text{m}$ , and, with reference to Fig. 3, the particle with elliptical cross section is characterized by the parameters  $\theta_R = 0^\circ$  and  $T = 0.25 \mu\text{m}$ . For the sinusoidally perturbed particle, amplitude  $h = 0.05 \mu\text{m}$  and constant  $f = 5$ , which implies that there are five cycles in the perimeter of the particle. At the fundamental frequency the particle with cylindrical cross section has more-pronounced oscillations than the perturbed particles. The perturbations seem to affect the sharpness, and even the presence, of the resonant peaks. As could be expected, the resonant behavior of the particle with cylindrical geometry is much more pronounced in the second-harmonic efficiency curve. For the other particles, the second-harmonic efficiency curves are rather featureless in this range.

The consequences of orienting the elliptically shaped particle in different ways are illustrated in Fig. 9. As in Fig. 8, the wavelength range is  $0.24 \mu\text{m} < \lambda < 0.31 \mu\text{m}$ ,  $R = 0.5 \mu\text{m}$ , and  $T = 0.25 \mu\text{m}$ . In the linear calcula-

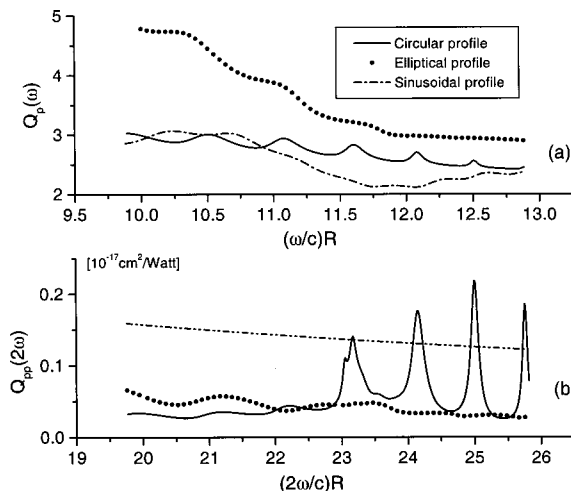


Fig. 8. Scattering cross sections for particles of different shapes illuminated with  $p$ -polarized light. (a) Fundamental frequency, (b) second-harmonic frequency. The three kinds of profile depicted in Fig. 3 are considered. The parameters are  $R = 0.5 \mu\text{m}$ ,  $T = 0.25 \mu\text{m}$ ,  $\theta_R = 0^\circ$ ,  $h = 0.05 \mu\text{m}$ , and  $f = 5$ .

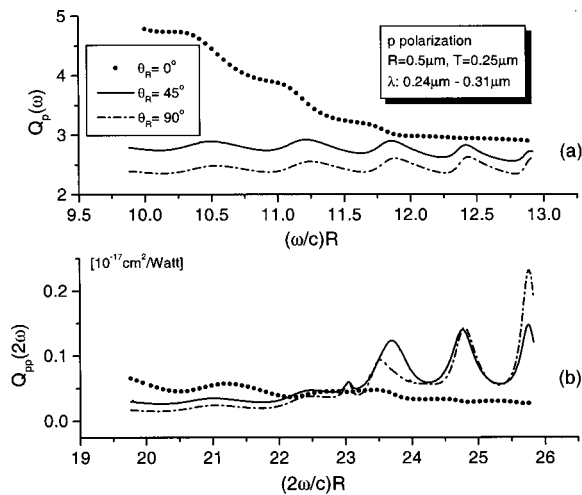


Fig. 9. Scattering cross sections for particles with elliptical geometrical cross section and different orientations illuminated with  $p$ -polarized light. (a) Fundamental frequency, (b) second-harmonic frequency. The orientations considered are  $\theta_R = 0^\circ$ ,  $\theta_R = 45^\circ$ , and  $\theta_R = 90^\circ$ . The parameters of the ellipse are  $R$  and  $T$ .

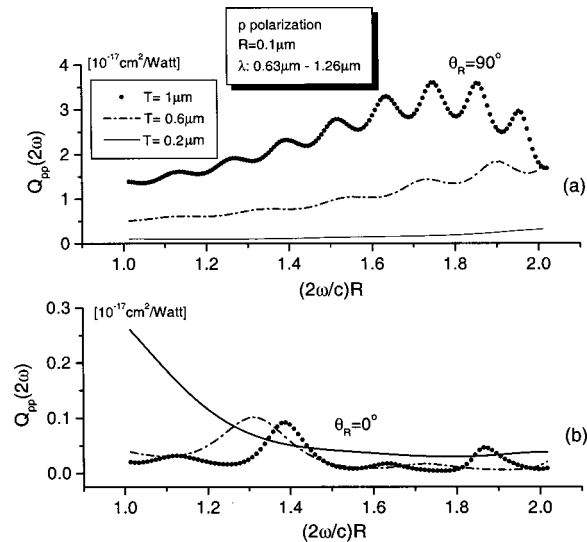


Fig. 10. Second-harmonic scattering cross sections for elliptical particles with different aspect ratios, illuminated with  $p$ -polarized light. Values of  $R$  and semiaxis  $T$  apply to both figures.

tions we can see that by rotating the particle it is possible to excite some resonance modes that do not coincide with the modes of the cylindrical particle. The excitation of these resonances is very clear in the second-harmonic efficiency, where they are more pronounced.

When the particle size is comparable to or larger than the wavelength, retardation effects of the incoming field across the particle can have a significant influence on the second-harmonic radiation. For example, one can expect important changes in the harmonic efficiency as the characteristic dimension of the particle is varied. These issues are explored in Fig. 10 for an elliptical particle with semiaxis  $R = 0.1 \mu\text{m}$ . Semiaxis  $T$  takes the values 0.2, 0.6, and  $1 \mu\text{m}$ . The figure shows calculations of the harmonic cross sections for  $p$ -polarized illumination in the wavelength range  $\lambda = 0.63\text{--}1.26 \mu\text{m}$ . Figure 10(a) is for

$\theta_R = 90^\circ$ , and Fig. 10(b) is for  $\theta_R = 0^\circ$ . We observe from Fig. 10 that retardation effects seem to be more important than the geometrical cross section of the particle. In particular, the maximum of Fig. 10(a) is  $\sim 15$  times higher than the maximum of Fig. 10(b).

The second-harmonic differential scattering cross sections for an ellipse with  $R = 0.5 \mu\text{m}$  and  $T = 0.25 \mu\text{m}$ , illuminated with  $p$ -polarized light of wavelength  $\lambda = 1.0 \mu\text{m}$ , are presented in Fig. 11. The two parts of Fig. 11 correspond to orientations with  $\theta_R = 0^\circ$  and  $\theta_R = 45^\circ$ . The strength of the lobes of the second-harmonic pattern is three times larger for  $\theta_R = 0^\circ$ . As expected, when the symmetry about the  $x_1$  axis is broken, some second-harmonic radiation is present in the forward-scattering and backscattering directions.

It is also interesting to explore the consequences of the plasmon resonance of the particle<sup>40,41</sup> for SHG. In Fig. 12 we present results for the scattering cross section of cylindrical and elliptical nanoparticles illuminated with  $p$ -polarized light in the region  $\lambda = 0.16\text{--}0.63 \mu\text{m}$ . The characteristic size of the particles is  $R = 10 \text{ nm}$ . In the calculations we use bulk dielectric constants and neglect

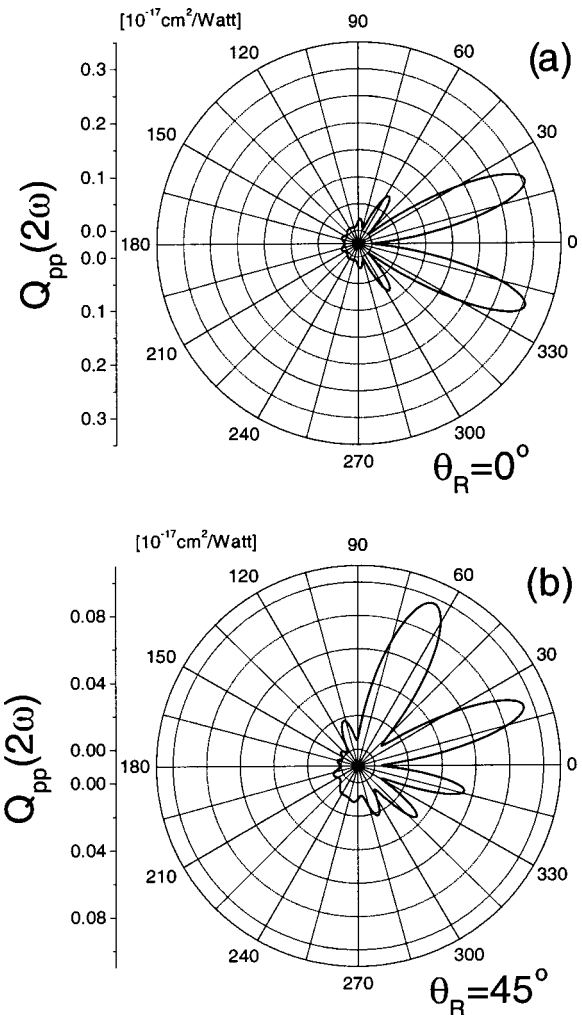


Fig. 11. Second-harmonic differential scattering cross sections for elliptical particles with different orientations illuminated with  $p$ -polarized light of wavelength  $\lambda = 1.0 \mu\text{m}$ . The parameters of the ellipse are  $R = 0.5 \mu\text{m}$  and  $T = 0.25 \mu\text{m}$ .

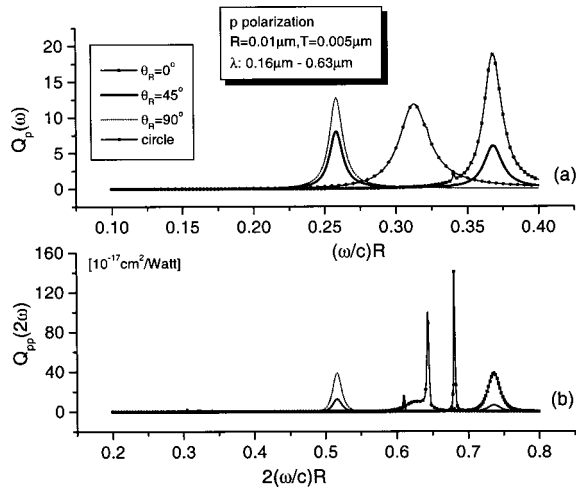


Fig. 12. Scattering cross sections for nanoparticles with circular and elliptical geometrical cross sections illuminated with  $p$ -polarized light. (a) Fundamental frequency, (b) second-harmonic frequency. A cylinder of radius  $R$  and ellipses with values of  $R$  and  $T$  are shown. Orientations considered are  $\theta_R = 0^\circ$ ,  $\theta_R = 45^\circ$ , and  $\theta_R = 90^\circ$ .

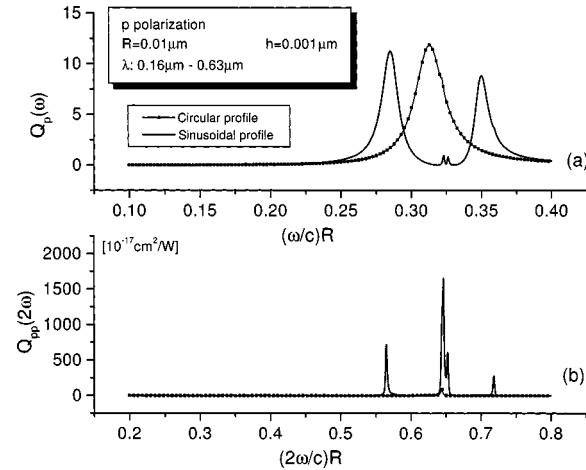


Fig. 13. Scattering cross sections for nanoparticles with circular and sinusoidally perturbed geometrical cross sections illuminated with  $p$ -polarized light. (a) Fundamental frequency, (b) second-harmonic frequency. A cylinder of radius  $R$  (solid curves) and a sinusoidally perturbed particle with  $h = 1$  nm (filled squares) are considered.

confinement effects on the nonlinear susceptibilities. Three orientations are considered for a particle with elliptical cross section with  $T = 5$  nm. At the fundamental frequency, the particle with circular cross section has a well-defined resonance centered on  $(\omega R/c) \approx 0.313$ , which corresponds to a wavelength  $\lambda = 200.93$  nm, for which  $\Re[\epsilon(\omega)] = -1.16$ . For the particle with elliptical cross section the resonance is split, and two modes appear. When the axes of symmetry of the ellipse lie along the  $x_1$  and  $x_3$  directions, only one of these modes is excited. However, for the ellipse with  $\theta_R = 45^\circ$ , the two modes are excited. These resonances are reflected in the second-harmonic cross section. It is worth pointing out, however, that the most prominent features of the second-harmonic cross section coincide with small, narrow features that are barely visible in the fundamental cross section. For the cylinder, this feature appears at  $(\omega R/c)$

$\approx 0.322$ , which corresponds to a wavelength  $\lambda = 195.29$  nm, at which  $\Re[\epsilon(\omega)] = -1.04$ . The two sharp modes on the second-harmonic efficiency that correspond to the particle with elliptical cross section are symmetrically located about the sharp resonance of the cylindrical particle.

Even small perturbations of the shapes of these two-dimensional nanoparticles have a profound effect on the particles' second-harmonic efficiency, as we illustrate in Fig. 13, where we compare the results for the cross section associated with a circular particle with those for a circular particle with a sinusoidal perturbation. The characteristic size of the particles is  $R = 10$  nm, and the amplitude of the perturbation is only  $h = 1$  nm. We can see that, at the fundamental frequency, whereas only one broad mode is excited in the cylindrical particle, two broad modes are visibly excited in the perturbed particle. The sharp features that are barely visible in the fundamental cross section have an important effect in the second harmonic cross section. In particular, we see that the largest resonance of the perturbed particle is 2 orders of magnitude higher than the resonances that correspond to the other particles. This condition could have important consequences in the design of nonlinear materials with nanoparticles.

## 6. SUMMARY AND CONCLUSIONS

We have described a numerical technique that is capable of dealing with second-harmonic generation in the interaction of light with arbitrary-shaped two-dimensional particles. Apart from the restrictions of the invariance of the particles along the  $x_2$  axis and the assumption of illumination perpendicular to this direction, the analysis is fairly general. It is based on the most general expression for nonlinear polarization for a centrosymmetric medium.

The expressions derived show that, on the one hand, one can produce  $p$ -polarized second-harmonic radiation by exciting the system with  $p$ - or  $s$ -polarized light. On the other hand,  $s$ -polarized second-harmonic radiation can be produced only by illumination of the cylinder with a combination of  $s$  and  $p$  polarized waves.

The theoretical results have been illustrated by examples for which the nonlinear susceptibilities were evaluated with a free-electron model. The method yields results that, for cylinders, are consistent with the results of analytical work. With  $p$ -polarized illumination, the scattering efficiency displays peaks that correspond to morphology-dependent resonances at the fundamental and harmonic frequencies. With  $s$  polarization, the linear response of the system is rather featureless, but some resonances appear in the second-harmonic radiation, which is  $p$  polarized.

An interesting general result is that, for particles that are symmetric about the illumination direction, there is no second-harmonic radiation along the forward-scattering and backscattering directions. We have also found that small perturbations in the profile of nanoparticles can have an important effect on the efficiency of second-harmonic generation.

## ACKNOWLEDGMENTS

C. I. Valencia is grateful to the Consejo Nacional de Ciencia y Tecnología for financial support through a Cátedra Patrimonial de Excelencia. This research was partially supported by a cooperative project funded by the Centro de Investigación Científica y de Educación Superior de Ensenada and the Centro de Investigaciones en Óptica, Mexico.

C. I. Valencia's e-mail address is [cvalenci@cicese.mx](mailto:cvalenci@cicese.mx).

## REFERENCES

- J. F. McGilp, "Optical characterization of semiconductor surfaces and interfaces," *Prog. Surf. Sci.* **49**, 1–106 (1995).
- Y. R. Shen, "Wave mixing spectroscopy for surface studies," *Solid State Commun.* **102**, 221–229 (1997).
- G. Lüpke, "Characterization of semiconductor interfaces by second-harmonic generation," *Surf. Sci. Rep.* **35**, 75–161 (1999).
- M. C. Downer, B. S. Mendoza, and V. I. Gavrilenko, "Optical second harmonic spectroscopy of semiconductor surfaces: advances in microscopic understanding," *Surf. Interface Anal.* **31**, 966–986 (2001).
- F. Brown, R. E. Parks, and A. M. Sleeper, "Nonlinear optical reflection from a metallic boundary," *Phys. Rev. Lett.* **14**, 1029–1031 (1965).
- F. Brown and R. E. Parks, "Magnetic-dipole contribution to optical harmonics in silver," *Phys. Rev. Lett.* **16**, 507–509 (1966).
- N. Bloembergen, R. K. Chang, and C. H. Lee, "Second harmonic generation of light in reflection from media with inversion symmetry," *Phys. Rev. Lett.* **16**, 986–989 (1966).
- N. Bloembergen, R. K. Chang, S. S. Jha, and C. H. Lee, "Optical second-harmonic generation in reflection from media with inversion symmetry," *Phys. Rev.* **174**, 813–822 (1968).
- J. Rudnick and E. A. Stern, "Second harmonic generation from metal surfaces," *Phys. Rev. B* **4**, 4274–4290 (1971).
- P. Guyot-Sionnest and Y. R. Shen, "Bulk contribution in surface second-harmonic generation," *Phys. Rev. B* **38**, 7985–7989 (1988).
- B. S. Mendoza and W. L. Mochán, "Exactly solvable model of surface second-harmonic generation," *Phys. Rev. B* **53**, 4999–5006 (1996).
- B. S. Mendoza and W. L. Mochán, "Erratum: Exactly solvable model of surface second-harmonic generation," *Phys. Rev. B* **53**, 4999 (1996).
- G. A. Farias and A. A. Maradudin, "Second harmonic generation in reflection from a metallic grating," *Phys. Rev. B* **30**, 3002–3012 (1984).
- R. T. Deck and R. K. Grygier, "Surface-plasmon enhanced harmonic generation at a rough metal surface," *Appl. Opt.* **23**, 3202–3213 (1984).
- J. L. Coutaz, M. Nevriere, E. Pic, and R. Reinisch, "Experimental study of surface-enhanced second-harmonic generation on silver gratings," *Phys. Rev. B* **32**, 2227–2232 (1985).
- A. R. McGurn, V. M. Agranovich, and T. A. Leskova, "Weak-localization effects in the generation of second harmonics of light at a randomly rough vacuum-metal grating," *Phys. Rev. B* **44**, 11441–11456 (1991).
- K. A. O'Donnell, R. Torre, and C. S. West, "Observations of backscattering effects in second-harmonic generation from a weakly rough metal surface," *Opt. Lett.* **21**, 1738–1740 (1996).
- K. A. O'Donnell, R. Torre, and C. S. West, "Observations of second-harmonic generation from randomly rough metal surface," *Phys. Rev. B* **55**, 7985–7992 (1997).
- K. A. O'Donnell and R. Torre, "Second-harmonic generation from strongly rough metal surfaces," *Opt. Commun.* **138**, 341–344 (1997).
- M. Leyva-Lucero, E. R. Méndez, T. A. Leskova, A. A. Maradudin, and J. Q. Lu, "Multiple scattering effects in the second harmonic generation of light in reflection from a randomly rough metal surface," *Opt. Lett.* **21**, 1809–1811 (1996).
- M. A. Leyva-Lucero, E. R. Méndez, T. A. Leskova, and A. A. Maradudin, "Destructive interference effects in the second harmonic light generated at randomly rough metal surfaces," *Opt. Commun.* **161**, 79–94 (1999).
- X. M. Hua and J. I. Gersten, "Theory of second harmonic generation by small metal spheres," *Phys. Rev. B* **33**, 3756–3764 (1986).
- D. Rogovin and T. P. Shen, "Microparticle surface-enhanced second-harmonic generation," *J. Opt. Soc. Am. B* **5**, 1886–1889 (1988).
- K. Hayata and M. Koshihara, "Theory of surface-emitting second-harmonic generation from optically trapped microspheres," *Phys. Rev. A* **46**, 6104–1889 (1992).
- J. Martorell, R. Vilaseca, and R. Crobalán, "Scattering of second-harmonic light from small spherical particles ordered in a crystalline lattice," *Phys. Rev. A* **55**, 4520–4525 (1997).
- J. I. Dadap, J. Shan, K. B. Eisenthal, and T. F. Heinz, "Second-harmonic Rayleigh scattering from a sphere of centrosymmetric material," *Phys. Rev. Lett.* **83**, 4045–4048 (1999).
- V. L. Brudny, B. S. Mendoza, and W. L. Mochán, "Second-harmonic generation from spherical particles," *Phys. Rev. B* **62**, 11152–11162 (2000).
- R. W. Boyd, *Nonlinear Optics* (Academic, New York, 1992).
- J. E. Sipe and G. I. Stegeman, "Nonlinear optical response of metal surfaces," in *Surface Polaritons*, V. M. Agranovich and D. L. Mills, eds. (North-Holland, Amsterdam, 1982), pp. 661–701.
- Y. R. Shen, *The Principles of Nonlinear Optics* (Wiley, New York, 1984), p. 10.
- D. Maystre, M. Nevriere, and R. Reinisch, "Nonlinear polarization inside metals: a mathematical study of the free electron model," *Appl. Phys. A* **39**, 115–121 (1986).
- C. I. Valencia, E. R. Méndez, and B. S. Mendoza, "Second-harmonic generation in the scattering of light by an infinite cylinder," submitted to *J. Opt. Soc. Am. B*.
- E. Born and E. Wolf, *Principles of Optics*, 7th ed. (Cambridge U. Press, Cambridge, 1999), p. 638.
- A. Mendoza-Suárez and E. R. Méndez, "Light scattering by reentrant fractal surfaces," *Appl. Opt.* **36**, 3521–3531 (1997).
- C. I. Valencia and R. A. Depine, "Resonant scattering of light by an open cylindrical cavity ruled on a highly conducting flat surface," *Opt. Commun.* **159**, 254–265 (1999).
- A. A. Maradudin, T. Michel, A. R. McGurn, and E. R. Méndez, "Enhanced backscattering of light from a random grating," *Ann. Phys. (N.Y.)* **203**, 255–307 (1990).
- M. Abramowitz and I. A. Stegun, *Handbook of Mathematical Functions* (Dover, New York, 1970), p. 364.
- P. B. Johnson and R. W. Christy, "Optical constants of the noble metals," *Phys. Rev. B* **6**, 4370–4379 (1972).
- S. C. Hill and R. E. Benner, "Morphology-dependent resonances," in *Optical Effects Associated with Small Particles*, P. W. Barber and R. K. Chang, eds. (World Scientific, Singapore, 1988), pp. 3–61.
- J. P. Kottmann, O. J. F. Martin, D. R. Smith, and S. Schultz, "Non-regularly shaped plasmon resonant nanoparticle as localized light source for near field microscopy," *J. Microsc.* (Oxford) **202**, 60–65 (2000).
- J. P. Kottmann, O. J. F. Martin, D. R. Smith, and S. Schultz, "Dramatic localized electromagnetic enhancement in plasmon resonant nanowires," *Chem. Phys. Lett.* **341**, 1–6 (2001).